

Article

Influences of Co-Content on the Physico-Chemical and Catalytic Properties of Perovskite $\text{GdCo}_x\text{Fe}_{1-x}\text{O}_3$ in CO Hydrogenation

Elizaveta M. Borodina ¹, Liliya V. Yafarova ², Tatiana A. Kryuchkova ¹, Tatiana F. Sheshko ^{1,*} ,
Alexander G. Cherednichenko ¹ and Irina A. Zvereva ^{2,*} 

¹ Department of Physical and Colloidal Chemistry, Faculty of Science, Peoples' Friendship University of Russia (RUDN University), 6 Miklukho-Maklaya Street, 117198 Moscow, Russia

² Department of Chemical Thermodynamics and Kinetics, Institute of Chemistry, Saint Petersburg State University, 7/9 Universitetskaya nab., 199034 Saint Petersburg, Russia

* Correspondence: sheshko-tf@rudn.ru (T.F.S.); irina.zvereva@spbu.ru (I.A.Z.); Tel.: +7-49-5955-0766 (T.F.S.); +7-90-4330-5019 (I.A.Z.)

Abstract: The effect of the substitution of cobalt into the GdFeO_3 perovskite structure on the selective hydrogenation of CO was investigated. A series of $\text{GdCo}_x\text{Fe}_{1-x}\text{O}_3$ ($x = 0; 0.2; 0.5; 0.8; 1$) samples were synthesized by sol-gel technology and characterized by XRD, BET specific area, DSC, TG, EDX and XPS. The experimental data made it possible to reveal a correlation between the state of iron and cobalt atoms, the fractions of surface and lattice oxygen, and catalytic characteristics. It has been found that varying the composition of $\text{GdCo}_x\text{Fe}_{1-x}\text{O}_3$ complex oxides leads to a change in the oxygen-metal binding energy in Gd-O-Me, the ratio of metals in various oxidation states, and the amount of surface and lattice oxygen, which affects the adsorption and catalytic characteristics of complex oxides.

Keywords: heterogeneous catalysis; CO hydrogenation; light olefins; syngas; perovskite; complex oxides



Citation: Borodina, E.M.; Yafarova, L.V.; Kryuchkova, T.A.; Sheshko, T.F.; Cherednichenko, A.G.; Zvereva, I.A. Influences of Co-Content on the Physico-Chemical and Catalytic Properties of Perovskite $\text{GdCo}_x\text{Fe}_{1-x}\text{O}_3$ in CO Hydrogenation. *Catalysts* **2023**, *13*, 8. <https://doi.org/10.3390/catal13010008>

Academic Editor: Guillermo Ahumada

Received: 27 November 2022

Revised: 16 December 2022

Accepted: 19 December 2022

Published: 22 December 2022



Copyright: © 2022 by the authors. Licensee MDPI, Basel, Switzerland. This article is an open access article distributed under the terms and conditions of the Creative Commons Attribution (CC BY) license (<https://creativecommons.org/licenses/by/4.0/>).

1. Introduction

Light olefins are among the basic petrochemical products. Currently, the global production of these products is estimated at 185 million tons [1], and the global production of propylene already exceeds 100 million tons per year [2]. The continuous growth in demand for light olefins is largely determined by the increase in the consumption of polyethylene and polypropylene and the expansion of their technological applications. To solve this problem, it is necessary to create a variety of effective catalytic technologies to produce light olefins from available raw materials.

One of the promising methods of ethylene production is the process of hydrogenation of CO. This process implies the use of noble metal-based catalysts such as Ru, Pt, Pd and Rh because of their inherent resistance to carbon deposition on the surface. However, the use of these catalysts is not economically viable. The industry also prefers nickel and cobalt catalysts because these metals are inexpensive and readily available. However, nickel- and cobalt-based catalysts are more prone to coke deposition under these synthesis conditions, resulting in reduced activity and deactivation [3–5].

Thus, the development of low-budget, effective and sintering-resistant catalysts for obtaining ethylene is an important problem. The issue of studying and developing new catalytic systems, improving already used processes and creating new methods aimed at obtaining olefins under conditions of hydrogenation of carbon monoxide remains relevant nowadays. Oxides with a perovskite structure (ABO_3) are considered an alternative to traditional catalysts for many industrial processes due to their high thermal stability, the ability to control physicochemical properties and low cost [6–8]. One of the advantages of perovskite-like oxides is the possibility of creating a wide range of compositions by complete/partial, as well as isovalent/non-isovalent substitution of A and B cations

while maintaining the structure. This allows for controlling the stability of the structure [9], electronic [10], redox and surface properties of complex oxides [11], creating new functional materials [12–20].

Perovskites have good flexibility and diversity in their chemical composition and can accommodate solid defects, such as vacancies at both the cation and anion sites [21], [22]. The B-site transition metals on the surface are believed to be the active centers owing to the exposed 3d electron orbitals. Considering that the B-site transition metals embedded in the perovskite lattice are atomically dispersed, we can expect to develop highly active and anti-coking catalysts.

Perovskites have been widely studied in oxidation reactions [23–25]. However, the study of Fe- and Co-containing perovskites in the hydrogenation of carbon monoxide is insufficiently described in the literature [26–31]. From the analysis of the existing works, it can be concluded that there is a close relationship between the nature and chemical state of the elements responsible for the activity and the type of surface C-containing intermediates and product distributions. Accordingly, A(Fe/Co)O₃ perovskite-type oxides with reducible B³⁺ ions under typical reaction conditions are excellent model catalysts for gaining new and useful insight into the surface process taking place during CO activation and carbon chain growth.

Thereby the purpose of this work was to study the catalytic activity of systems based on perovskite-type iron- and cobalt-containing complex oxides in the process of carbon monoxide hydrogenation and to establish the relationship between the physicochemical properties of complex oxides and their catalytic characteristics. It should be noted that catalysts of similar composition worked well for dry reforming of methane [32] and diesel soot oxidation [33].

2. Results and Discussion

2.1. Characterization

Complex oxides GdCo_xFe_{1-x}O₃ ($x = 0; 0.2; 0.5; 0.8; 1$) were studied by X-ray phase analysis, X-ray photoelectron spectroscopy and SEM+EDX. Detailed XFA and XPS results are presented in [26]. All samples are single-phase and have an orthorhombic structure with the spatial group *Pbnm* and *Pnma*. All diffraction peaks can be attributed to the orthorhombic structure of GdFeO₃ (PDF-ICDD 01-072-9908), GdCoO₃ (PDF-ICDD 00-025-1057) and their solid solutions.

Analysis of the dependence of the structural parameters *a*, *b* and *c* on the composition of GdCo_xFe_{1-x}O₃ ($x = 0; 0.2; 0.5; 0.8; 1$) (Figure 1) shows that the values of parameters *a* and *c* decrease slightly with a greater iron substitution for cobalt in ferrite, while the lattice parameter *b* remains practically unchanged for all complex oxides except for the ferrite samples with cobalt fraction $x = 0.8$ and completely substituted GdCoO₃. This indicates that the lattice geometry distorts with increasing cobalt content.

The crystallite size of the obtained samples estimated using the Scherrer formula is in the range from ~47 to 65 nm (Table 1) and does not show a dependence on the composition [33].

The specific surface area of the obtained compounds was determined by the BET method (Table 1); for GdFeO₃, the highest value was observed, which is consistent with the results of scanning electron microscopy. For gadolinium cobaltite and solid solutions GdCo_xFe_{1-x}O₃ ($x = 0.2; 0.5; 0.8$), the low values of the specific surface area are due to the relatively high calcination temperature (800 °C). At the same time, the values of the surface area of the obtained oxides were found to be higher than for similar compounds prepared by the ceramic method (less than 1.0 m²/g) [34]. Thus, the values of the specific surface area do not show a dependence on the composition, and the conditions of preparation have a great influence.

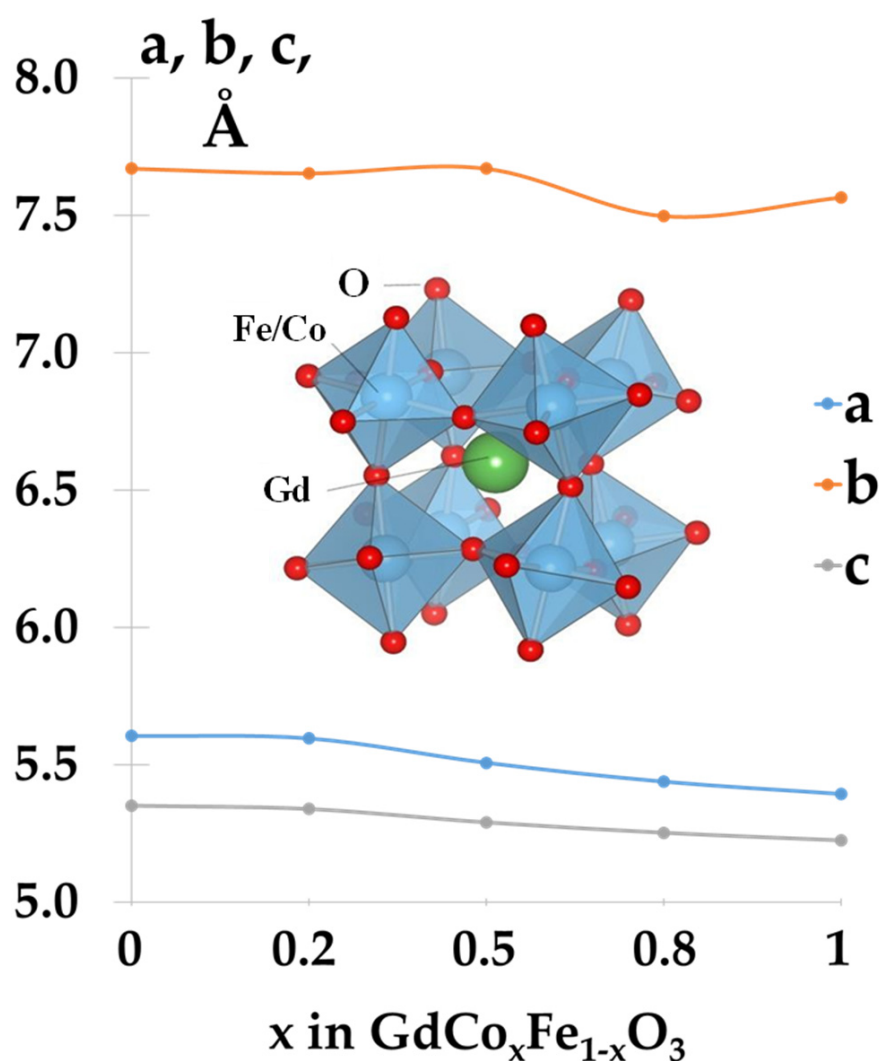


Figure 1. Dependence of structural parameters a , b and c on composition $\text{GdCo}_x\text{Fe}_{1-x}\text{O}_3$ ($x = 0; 0.2; 0.5; 0.8; 1$).

Table 1. Results of studying $\text{GdCo}_x\text{Fe}_{1-x}\text{O}_3$ ($x = 0; 0.2; 0.5; 0.8; 1$) surface composition by X-ray spectral, microanalysis, XRD crystallite size and S_{BET} .

Compound	XRD Crystallite Size, nm	S_{BET} (m^2/g)	Content (at %)				Fe/Co
			Gd	Fe	Co	O	
GdFeO_3	53.4	9.9	18.53	19.15	-	62.32	-
$\text{GdCo}_{0.2}\text{Fe}_{0.8}\text{O}_3$	47.3	3.3	17.58	16.35	4.67	61.40	3.5
$\text{GdCo}_{0.5}\text{Fe}_{0.5}\text{O}_3$	50.5	2.7	17.43	8.77	9.49	64.31	0.92
$\text{GdCo}_{0.8}\text{Fe}_{0.2}\text{O}_3$	65.2	3.1	16.84	3.96	17.21	61.98	0.23
GdCoO_3	59.9	2.3	16.02	-	17.80	66.18	-

The surface morphology of gadolinium ferrite and cobaltite, as well as their solid solutions obtained after calcining at $800\text{ }^\circ\text{C}$ for 1 h, was studied using scanning electron microscopy. Figure 2 shows photomicrographs of the surface of oxides with the composition $\text{GdCo}_x\text{Fe}_{1-x}\text{O}_3$ ($x = 0; 0.2; 0.5; 0.8; 1$); all studied compounds demonstrate a similar surface morphology, which indicates that the complete or partial substitution of iron for cobalt in the perovskite structure does not affect surface morphology.

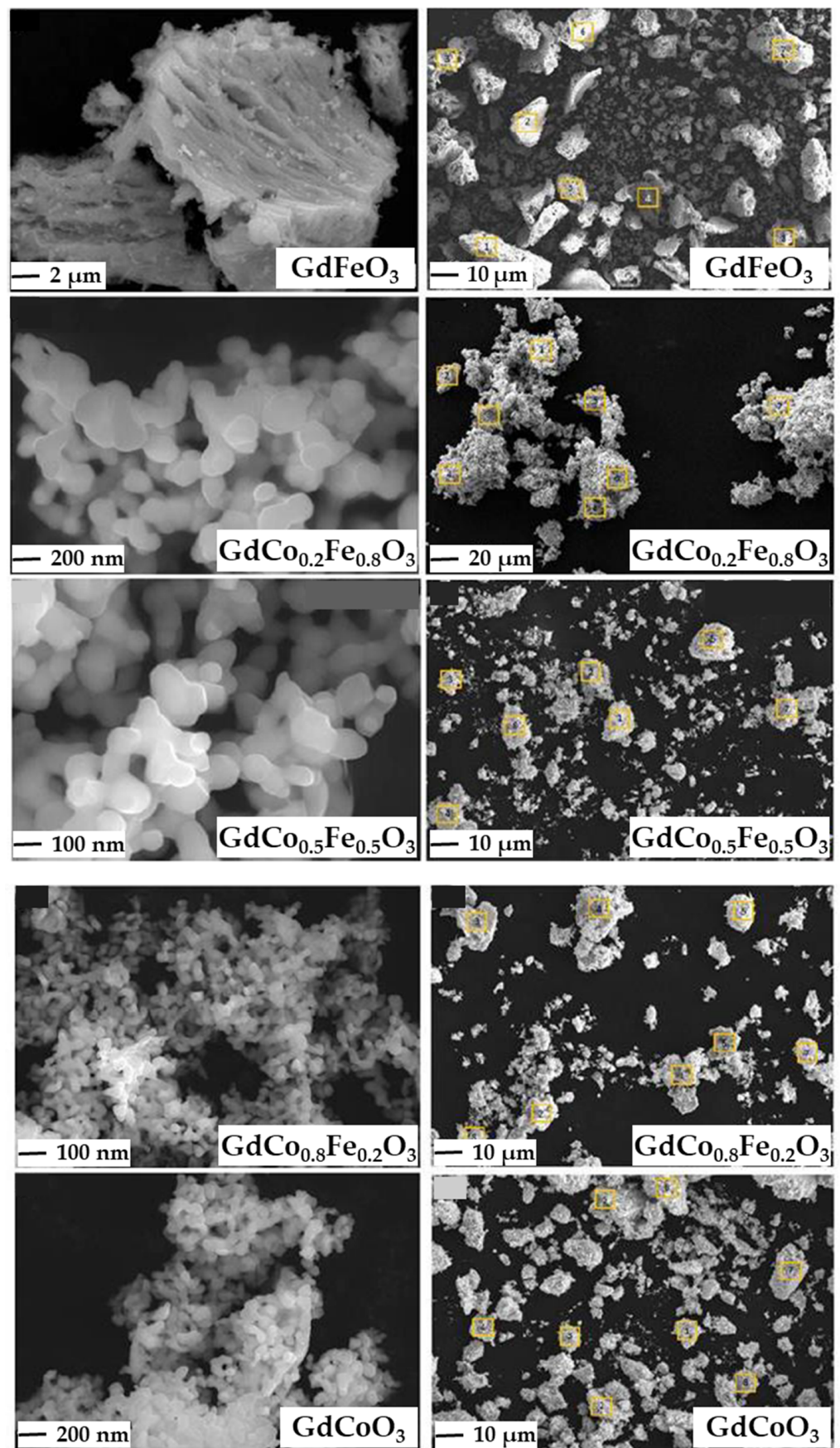


Figure 2. Micrographs of the surface of $\text{GdCo}_x\text{Fe}_{1-x}\text{O}_3$ ($x = 0; 0.2; 0.5; 0.8; 1$).

The micrographs of the surface in Figure 2 show a uniform morphology without particle agglomeration. The surface is characterized by a “porous” structure, possibly associated with combustion and gas evolution during oxide production. It should be noted that, in contrast to gadolinium cobaltite and partially substituted ferrites, gadolinium ferrite (GdFeO_3) exhibits a more porous morphology, which is due to a lower preparation temperature and is consistent with the results of determining the specific surface area (Table 1).

To study the composition of the surface, X-ray spectral analysis was used and elemental mapping of the surface was carried out. The results show that the amount of Gd and Fe/Co on the surface of the obtained compounds is close to the theoretical value (Table 1).

XPS was used to study the surface composition, the oxidation state and the distribution of atoms in the obtained compounds. Traditional photoelectron spectroscopy is a surface-sensitive method in which the depth of probing in the energy range 200 eV–1500 eV does not exceed 2 nm. Figure 3 presents the overview XPS spectra of oxides $\text{GdCo}_x\text{Fe}_{1-x}\text{O}_3$ ($x = 0; 0.2; 0.5; 0.8; 1$) in the binding energy range of 0–1400 eV and represents the intense peaks of Gd3d, Fe2p, Co2p, O1s and C1s (signals of other elements were not found). The chemical states of the atoms in the compounds under study were refined by decomposing the obtained spectra described in [33].

The partial substitution of iron for cobalt in the samples $\text{GdCo}_x\text{Fe}_{1-x}\text{O}_3$ ($x = 0.2; 0.5; 0.8$) resulted in the heterovalent state Fe^{2+} , Fe^{3+} (711.0; 724.0 eV) and $\text{Co}^{2+}/\text{Co}^{3+}$ (779.97; 794.0 eV) (Table 2). The heterovalent state causes the appearance of oxygen vacancies in the structure of Co-containing samples and changes in the bond lengths Me-O-Me [35].

Table 2. Results of studying the surface composition and state of atoms by XPS [33].

Compound	Fe	Co	Ratio		
			$\text{Co}^{2+}/\sum \text{Co}^{n+}$	$\text{Fe}^{2+}/\text{Fe}^{2+} + \text{Fe}^{3+}$	O_s/O_l
GdFeO_3	+3	-	-	0.64	1.52
$\text{GdCo}_{0.2}\text{Fe}_{0.8}\text{O}_3$	+2; +3	+2; +3	0.51	0.43	0.59
$\text{GdCo}_{0.5}\text{Fe}_{0.5}\text{O}_3$	+2; +3	+2; +3	0.50	0.58	0.81
$\text{GdCo}_{0.8}\text{Fe}_{0.2}\text{O}_3$	+2; +3	+2; +3	0.13	0.58	0.82
GdCoO_3	-	+2; +3	0.47	-	0.83

The O1s photoelectron spectra of compounds $\text{GdCo}_x\text{Fe}_{1-x}\text{O}_3$ ($x = 0; 0.2; 0.5; 0.8; 1$) shown in Figure 4 are asymmetric and wide, which confirms the presence of various types of oxygen in these compounds [36,37]. Analysis and decomposition of the spectra showed that the obtained compounds contained various types of oxygen (at binding energies of ~533.00 eV, 530.90 and 528.57–529.67 eV), which are referred to as physically adsorbed oxygen (H_2O), chemically adsorbed oxygen ($\text{O}_s:\text{O}_2^-$, O_2^{2-} and O^-) and lattice oxygen (O_l), respectively. Table 2 presents a quantitative assessment of various types of oxygen in the studied oxides. The O_s/O_l ratio in $\text{GdCo}_x\text{Fe}_{1-x}\text{O}_3$ at $x = 0.2; 0.5; 0.8; 1$ increases with an increase in the amount of cobalt, and these four samples have almost the same values of the surface area. At the same time, for the GdFeO_3 ($x = 0$), a higher value of the surface area and a higher value of the O_s/O_l ratio are observed. The study [38] shows that chemisorbed oxygen (O_s) plays an important role in low-temperature oxidative reactions, while lattice oxygen (O_l) affects the oxidizing ability of compounds in high-temperature reactions. Thus, the O_s/O_l ratio can be used to assess the oxidative characteristics of the compounds under study.

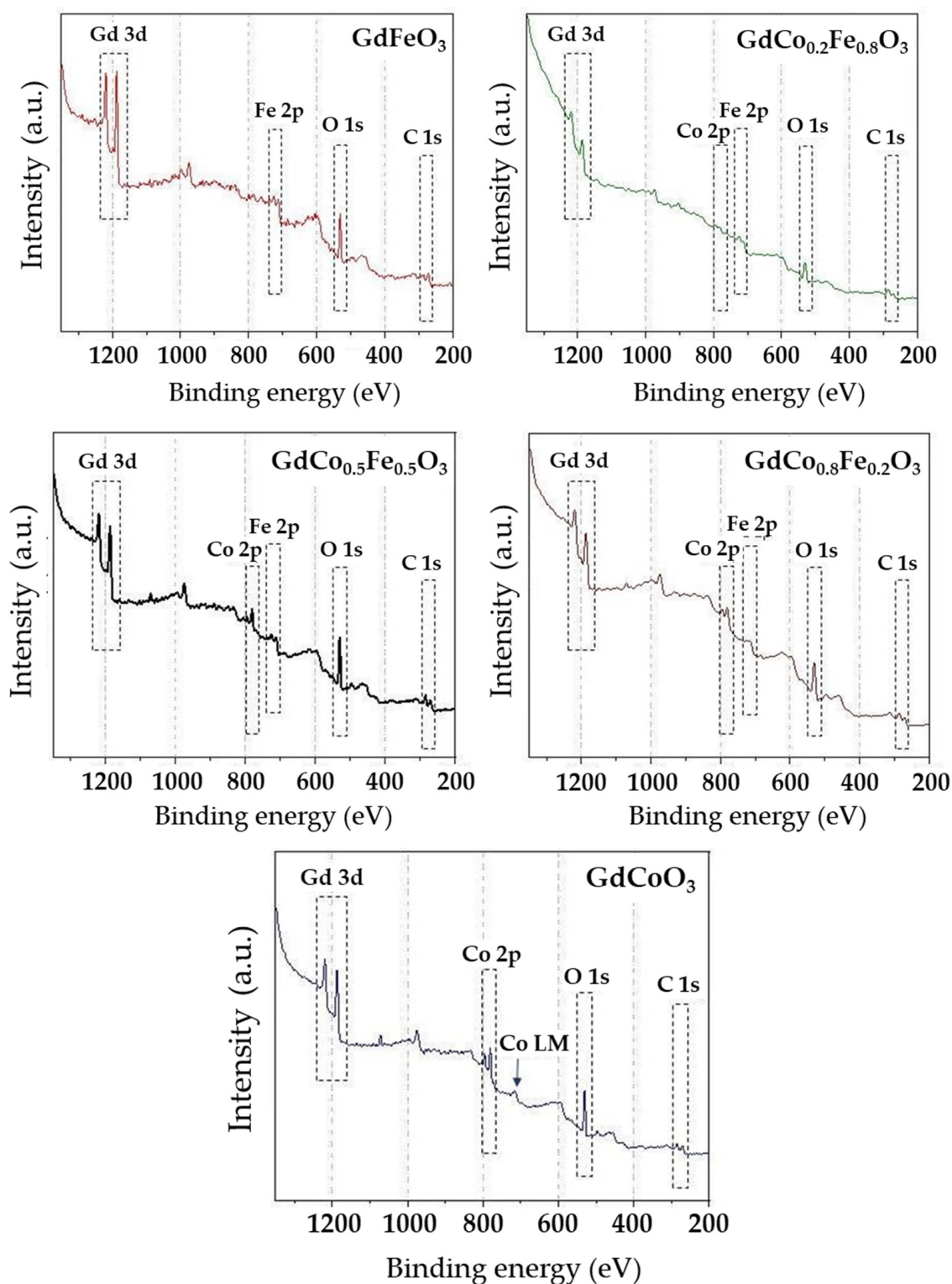


Figure 3. Survey XPS spectrum for compounds in the composition $\text{GdCo}_x\text{Fe}_{1-x}\text{O}_3$ ($x = 0; 0.2; 0.5; 0.8; 1$) and identification of the main photoelectron lines.

As was shown in [33], when using the H_2 -TPR and O_2 -TPD methods, the mobility of lattice oxygen increases with increasing cobalt content in $\text{GdCo}_x\text{Fe}_{1-x}\text{O}_3$ samples. This tendency confirmed that there are a large number of cationic vacancies in the Co-rich samples due to the easier $\text{Co}^{3+} \rightarrow \text{Co}^{2+}$ transition.

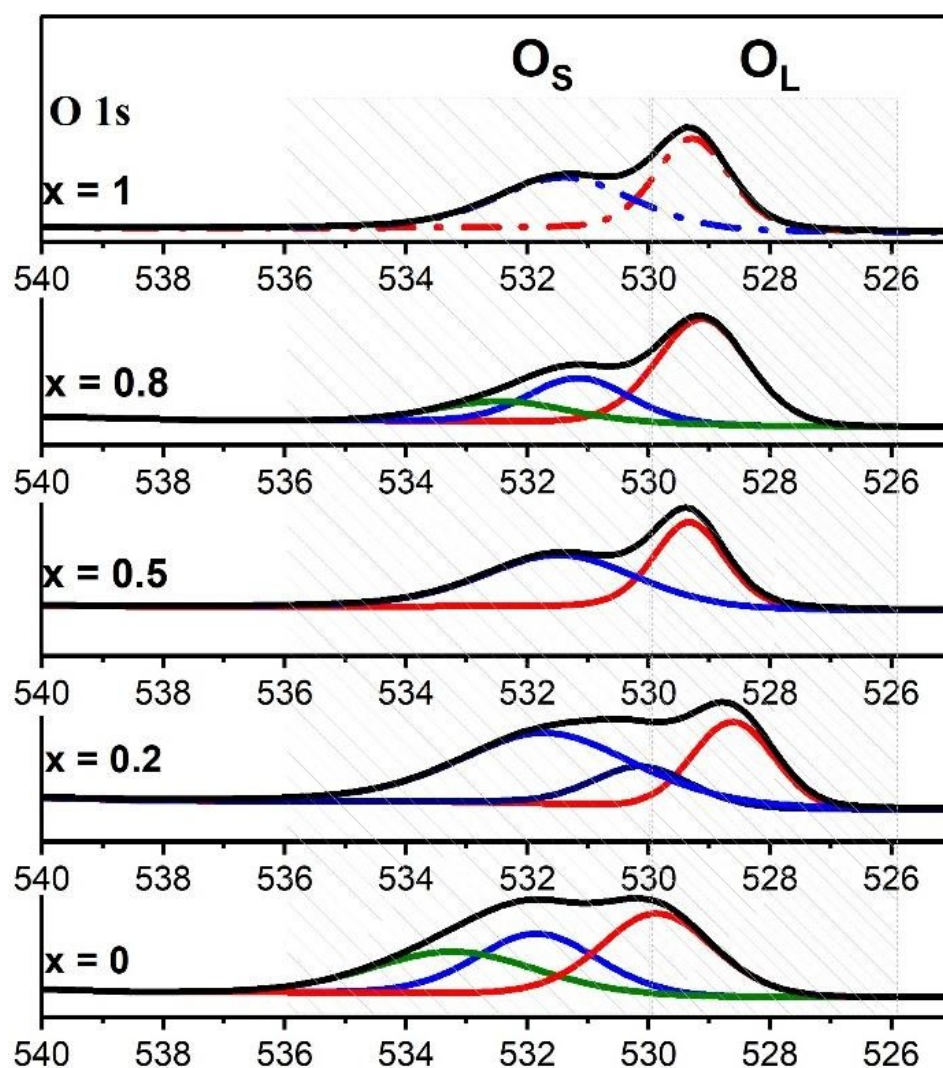


Figure 4. O1s spectra for compounds $\text{GdCo}_x\text{Fe}_{1-x}\text{O}_3$ ($x = 0; 0.2; 0.5; 0.8; 1$) [33].

2.2. CO Hydrogenation

The catalytic activity in the reaction of carbon monoxide hydrogenation was evaluated in the temperature range 523–708 K at a $\text{CO}:\text{H}_2$ ratio = 1:2 (CO conversions are shown in Figure 5). The substitution of small amounts of cobalt ($x < 0.5$) led to the suppression of CO conversions compared to the initial gadolinium ferrite. On the sample $\text{GdCo}_{0.2}\text{Fe}_{0.8}\text{O}_3$ ($x = 0.8$), degrees of conversion of carbon monoxide did not exceed 45%. Substitution of iron for cobalt ($x = 0.2; 0.5$) leads to an improvement in oxygen mobility and a decrease in the amount of surface oxygen O_s . This is reflected in the decrease in CO conversion as CO is adsorbed through the surface oxygen, but the introduction of more cobalt into ferrite gadolinium ($x > 0.5$) promoted the growth of CO conversion and it reached 90–95%.

For $\text{GdCo}_x\text{Fe}_{1-x}\text{O}_3$ ($x = 0; 0.2; 0.5; 0.8$) samples, the conversions barely depended on temperature and reached almost maximum values at 523 K. This is due to the participation in the reaction of carbon particles formed because of the dissociative adsorption of CO at lower temperatures [21]. A slight increase in the CO conversion with increasing temperature may be due to the involvement of not only surface oxygen but lattice oxygen as well. The amount of CO in the gas phase correlated with its conversions and was determined by the type of catalyst. At the same time, on all catalysts, the process was accompanied by the formation of carbon dioxide, the amounts of which also depended on the composition of perovskite (Figure 6).

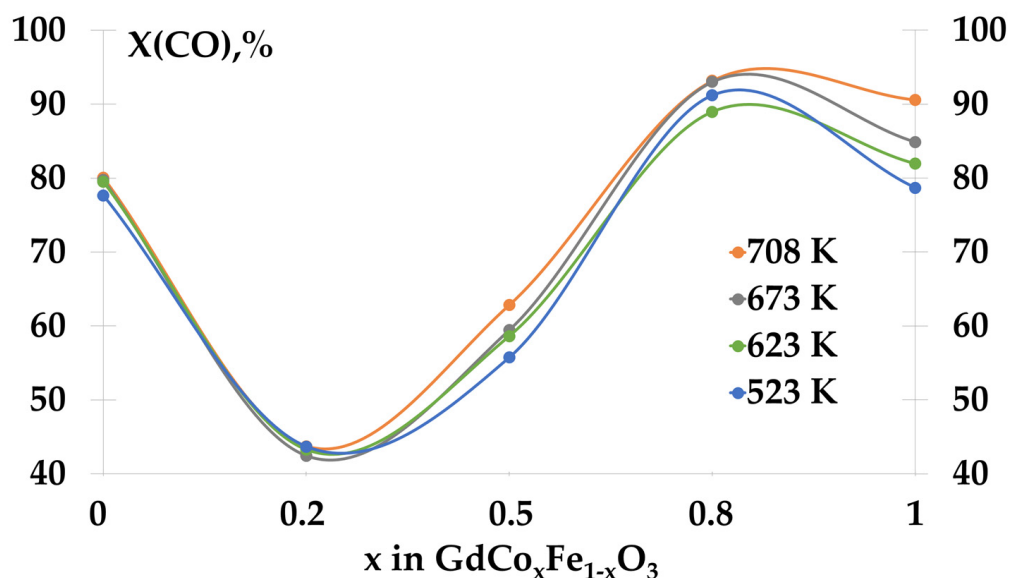


Figure 5. Temperature dependences of CO conversions when the reaction is carried out at a CO:H₂ = 1:2 ratio over GdCo_xFe_{1-x}O₃ (x = 0; 0.2; 0.5; 0.8, 1).

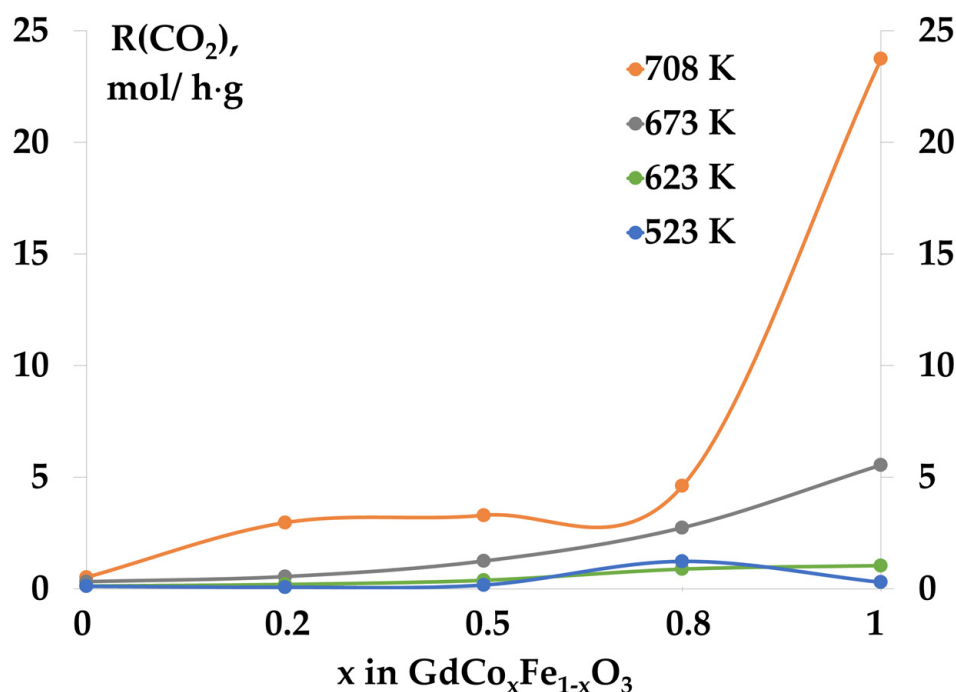


Figure 6. Temperature dependences of the CO₂ formation rates over GdCo_xFe_{1-x}O₃ complex oxides (CO:H₂ ratio = 1:2; GHSV = 8700 h⁻¹).

The amount of formed carbon dioxide in the region up to 623 K was approximately the same, but further increasing the temperature led to an increase in the rate of CO₂ formation. It should be noted that on the sample GdCoO₃, the process of CO₂ formation was much more intense than on the other samples.

It is known that CO adsorption mainly occurs at the A-centers of perovskite with the formation of carbonate complexes Gd₂O₂CO₃ [39]. The decomposition of these complexes produces carbon dioxide (Equation (1)).



In the studied perovskites, the parameters a and c of the crystal lattice change; hence, the oxygen-metal bond energy in Gd-O-Me will also change, which in turn leads to a change in the gadolinium-oxygen bond and is reflected in the value of CO adsorption. The formation of CO_2 is also possible in the interaction of the adsorbed CO_{ads} molecule with perovskite (O_S) oxygen (Equation (2)):



As stated above, the substitution of iron for cobalt improves oxygen mobility and redox properties and changes the ratio of surface and bulk oxygen in the structure of complex oxides: the share of O_S decreases, while the share of O_I increases. It can be assumed that with increasing temperatures, both surface and lattice oxygen begin to participate in the reaction (2) (the amount of lattice oxygen depends on the composition of the oxide, i.e., with cobalt enrichment the oxidation capacity of the samples increases).

The products of hydrogenation of carbon monoxide on $\text{GdCo}_x\text{Fe}_{1-x}\text{O}_3$ catalysts ($x = 0; 0.2; 0.5; 0.8; 1$) were C_1 – C_5 hydrocarbons, and the main ones were methane, ethylene, ethane and propylene. The rate of formation of hydrocarbons began at 573 K and increased with increasing temperatures.

A comparison of the rates of formation of the main products (methane, ethylene, propylene and CO_2) showed that the substitution of Fe in gadolinium ferrite for Co leads to an increase in the specific catalytic activity (Figure 7), but on the $\text{GdCo}_{0.2}\text{Fe}_{0.8}\text{O}_3$, a decrease in the rate of product formation was observed. It is worth noting that as the proportion of cobalt in the initial ferrite increases, the formation of propylene stops. The formation rates of methane and ethylene increased in the series:

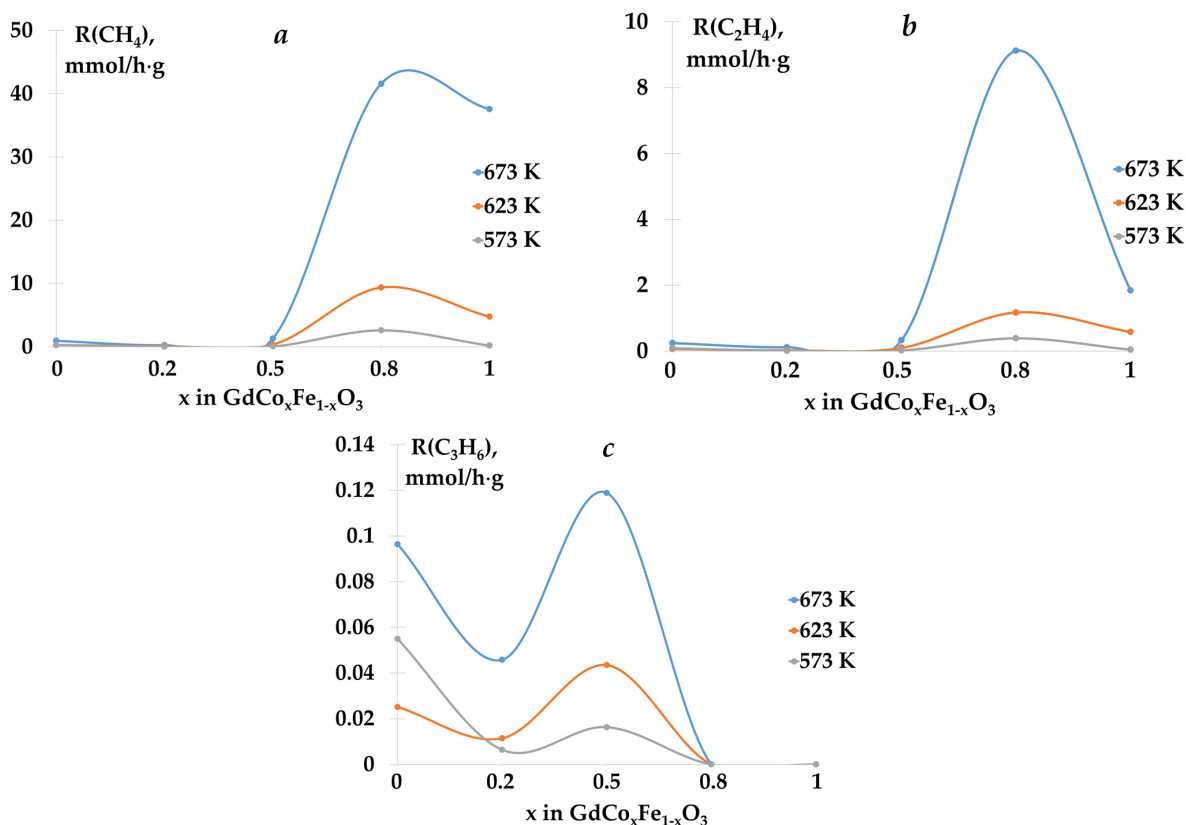


Figure 7. Temperature dependences of (a) methane, (b) ethylene and (c) propylene formation rates on $\text{GdCo}_x\text{Fe}_{1-x}\text{O}_3$ catalysts.

The appearance of a synergistic effect on $\text{GdCo}_{0.8}\text{Fe}_{0.2}\text{O}_3$ is due to the fact that this sample has different structural characteristics from the others.

Varying the composition of catalysts led to a change in the quantitative ratio of products. Thus, when performing the reaction on GdFeO_3 , the content of methane, ethylene and propylene at $T = 648 \text{ K}$ was 76%, 14% and 6%, respectively. The complete substitution of iron for cobalt increased the amount of methane to 85%. However, the $\text{GdCo}_{0.2}\text{Fe}_{0.8}\text{O}_3$ sample showed a decrease in methane to 38%, ethylene to 9% and propylene to 5%. The sample with the cobalt substitution fraction $x = 0.8$ had an ethylene content of 13%.

The dependence of the hydrocarbon chain growth factor α_i on the number of carbon atoms (i) in the chain of intermediate products is shown in Figure 8.

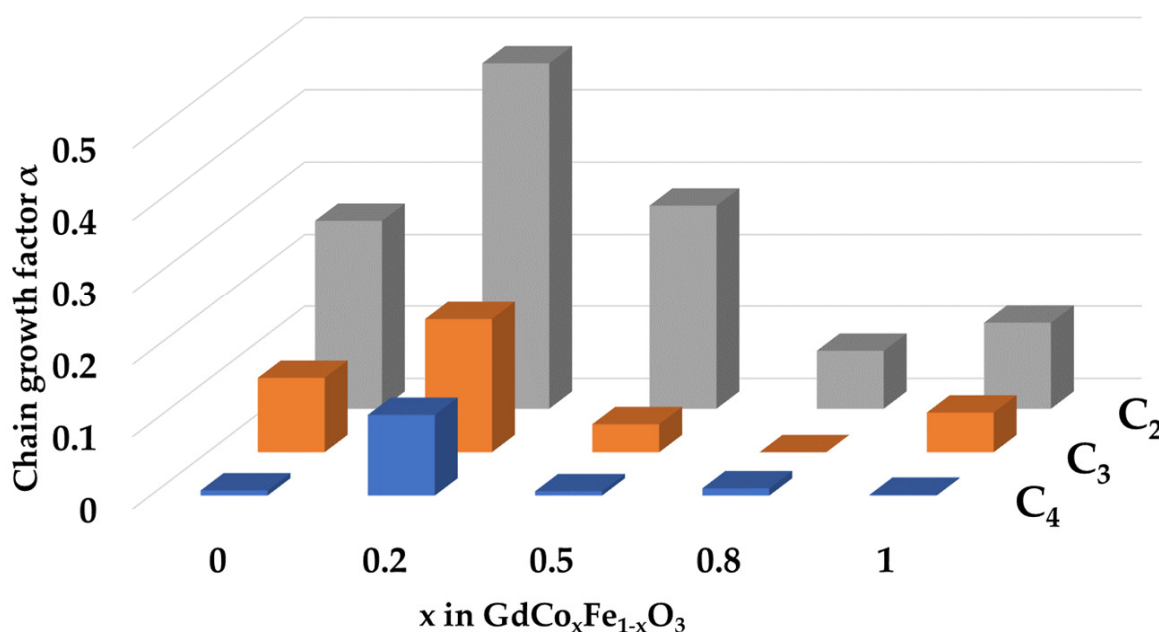


Figure 8. Chain growth factors α_i at 673 K for $i = 2, 3, 4$ over $\text{GdCo}_x\text{Fe}_{1-x}\text{O}_3$ catalysts.

Regardless of the catalyst composition, the highest values were for α_1 , i.e., the formation of hydrocarbons with two carbon atoms was most likely in the studied systems, and on the $\text{GdCo}_{0.2}\text{Fe}_{0.8}\text{O}_3$ catalyst, this probability reached a maximum of 50%.

From the literature data [35] it is known that iron hydrogen is adsorbed mainly in atomic form and molecular forms are practically absent, but cobalt hydrogen can be adsorbed in both atomic and molecular forms. Moreover, on the iron centers, hydrogen is more mobile relative to the surface, unlike cobalt, because in the series Fe, Co and Ni, bond energy Me-O grows [25,35]. Thus, increasing the proportion of cobalt in the B-position leads to the growth of the molecular forms of hydrogen and their ordering. The probability of the formation of CH_2 particles increases and results in the formation of hydrocarbons with an even number of carbon atoms.

The calculation of selectivity for target products (ethylene, propylene and butylene) showed that the substitution of iron for cobalt in the perovskite led to a decrease in selectivity for the target reaction products. Thus, at 573 K, the C_2^- - C_4^- selectivity on GdFeO_3 was 29% and 20% on GdCoO_3 (Figure 9). The replacement of iron with a small amount of cobalt led to an increase (of approximately 32%) in the selectivity of light olefins. The most selective with respect to ethylene turned out to be the sample with a fraction of cobalt $x = 0.2$, for which the $\text{Co}^{2+}/\sum \text{Co}^{n+}$ ratio is maximal and $\text{Fe}^{2+}/\sum \text{Fe}^{n+}$ is minimal.

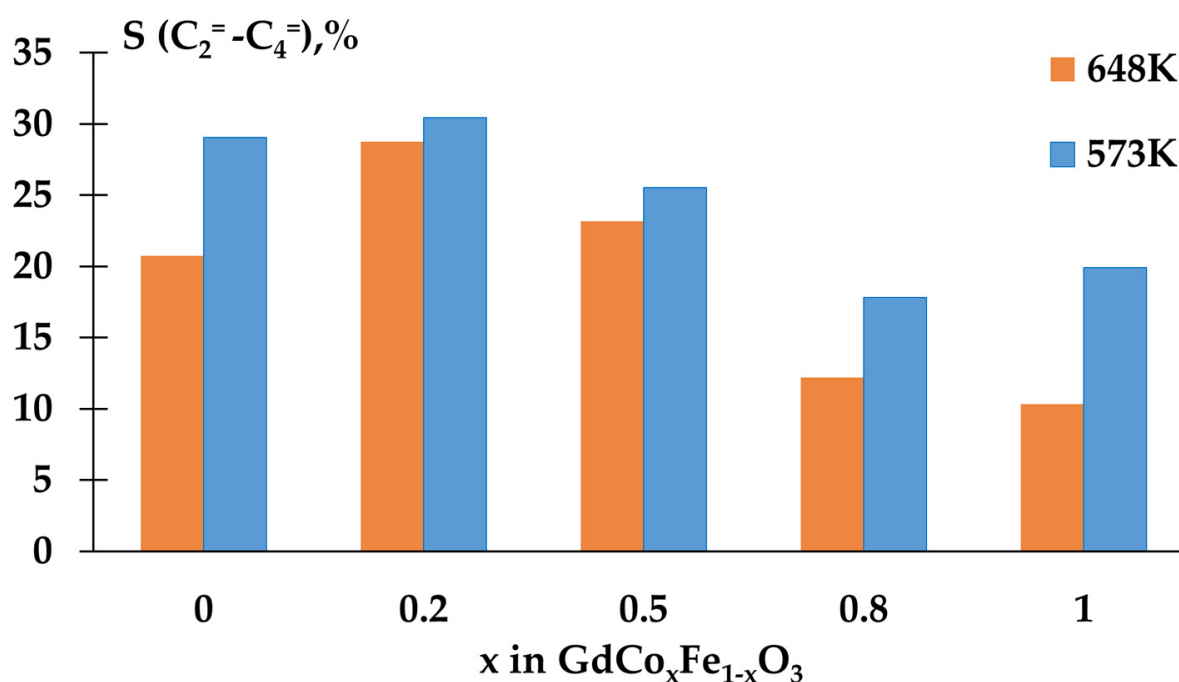


Figure 9. Temperature dependences of selectivity for light olefins over $\text{GdCo}_x\text{Fe}_{1-x}\text{O}_3$ catalysts.

To determine kinetic characteristics, such as the effective activation energies of product formation and the logarithms of the pre-exponential multiplier (an indirect characteristic of the number of the active centers of the catalyst surface), the interpolation of experimental data in linear coordinates of the Arrhenius equation was performed. On the Arrhenius dependences of the rates of formation of ethylene for samples with a content of cobalt $x > 0.5$ two areas of linearity with a transition temperature of about $T^* \approx 598\text{--}609.7\text{ K}$ were observed. The presence of two linear sections with different values of the activation energies E_a indicates either a change in the state of the active Me^{n+} centers depending on the temperature (change in the oxidation state of $\text{Co}^{3+} \leftrightarrow \text{Co}^{2+}$) or the course of different processes of a complex reaction in each temperature interval ($T < T^*$ is chemisorption of reactants, and $T > T^*$ is the conversion of chemisorbed complexes into products). The calculated values of the effective activation energies for the formation of reaction products and the logarithms of the prefactor for all the catalysts studied are shown in Table 3.

Table 3. Resulting atomic state, CO conversion, selectivity for olefins, experimental activation energies and pre-exponential multipliers for $\text{GdCo}_x\text{Fe}_{1-x}\text{O}_3$ catalysts.

Compound	GdFeO_3	$\text{GdCo}_{0.2}\text{Fe}_{0.8}\text{O}_3$	$\text{GdCo}_{0.5}\text{Fe}_{0.5}\text{O}_3$	$\text{GdCo}_{0.8}\text{Fe}_{0.2}\text{O}_3$	GdCoO_3
$\text{Co}^{2+} / \sum \text{Co}^{n+}$	-	0.52	0.50	0.13	0.47
$\text{Fe}^{2+} / \text{Fe}^{2+} + \text{Fe}^{3+}$	0.64	0.43	0.58	0.58	-
O_s / O_1	1.52	0.59	0.81	0.82	0.83
$\alpha(\text{CO}), \%$	80	44	63	93	89
$S(\text{C}_n\text{H}_{2n}), \%$	27.1	38.4	26.4	2.4	0.55
$E_a(\text{CH}_4), \text{kJ/mol}$	70	77	99	177/252	159
$\ln K_0(\text{CH}_4)$	5.7	5.6	11.3	29.6/46.6	25.1
R^2	0.96	0.97	0.99	0.99/0.99	0.99
$E_a(\text{C}_2\text{H}_4), \text{kJ/mol}$	112	88	115/186	112/244	99/226
$\ln K_0(\text{C}_2\text{H}_4)$	18.5	6.7	12.9/28.2	15.0/43.1	11.5/37.1
R^2	0.97	0.97	0.96/0.99	0.96/0.99	0.98/0.99

As the data in Table 3 show, the introduction of a small amount of cobalt led to a decrease in the activation energies of ethylene formation, while the value of the pre-exponential multiplier also decreased. The activation energies of methane formation and

the logarithms of the prefactor were comparable to those of the original ferrite. For the $\text{GdCo}_{0.8}\text{Fe}_{0.2}\text{O}_3$ sample, the effective activation energies were the highest. However, in spite of the high activation energy, high values of $\ln K_0$ are also observed. For the same sample, the minimum Co^{2+} content can be seen. For samples with a fraction of cobalt $x \geq 0.5$, there are comparable values of O_s/O_l and $\text{Fe}^{2+}/(\text{Fe}^{2+} + \text{Fe}^{3+})$, but only the samples with $x = 0.8$ the minimum $\text{Co}^{2+}/\sum \text{Co}^{n+}$ ratio and the highest rates of product formation were observed. At the same time, the most selective was the sample with the cobalt fraction $x = 0.2$, for which the $\text{Co}^{2+}/\sum \text{Co}^{n+}$ ratio is maximal and $\text{Fe}^{2+}/\sum \text{Fe}^{n+}$ is minimal.

It can be assumed that Co^{3+} and Fe^{3+} in the Gd-O-Me bond are active centers, and the presence of Co^{2+} somewhat complicates the process and shifts it towards the formation of olefins.

The determination of the deposited carbon on the surface of the catalytic systems because of the reaction was carried out by thermogravimetric analysis (TG) and differential scanning calorimetry (DSC). Figure 10 shows the mass loss curves for $\text{GdCo}_x\text{Fe}_{1-x}\text{O}_3$ samples ($x = 0; 0.5; 1$) as an example. In the temperature range of 553–593 K, a slight increase in the mass of the $\text{GdCo}_{0.5}\text{Fe}_{0.5}\text{O}_3$ sample was observed, which is most likely due to the process of oxygen chemisorption from the air environment on the surface carbon and the subsequent decrease in mass with exo-effects in the 573–753 K range is due to carbon desorption in the form of CO_2 .

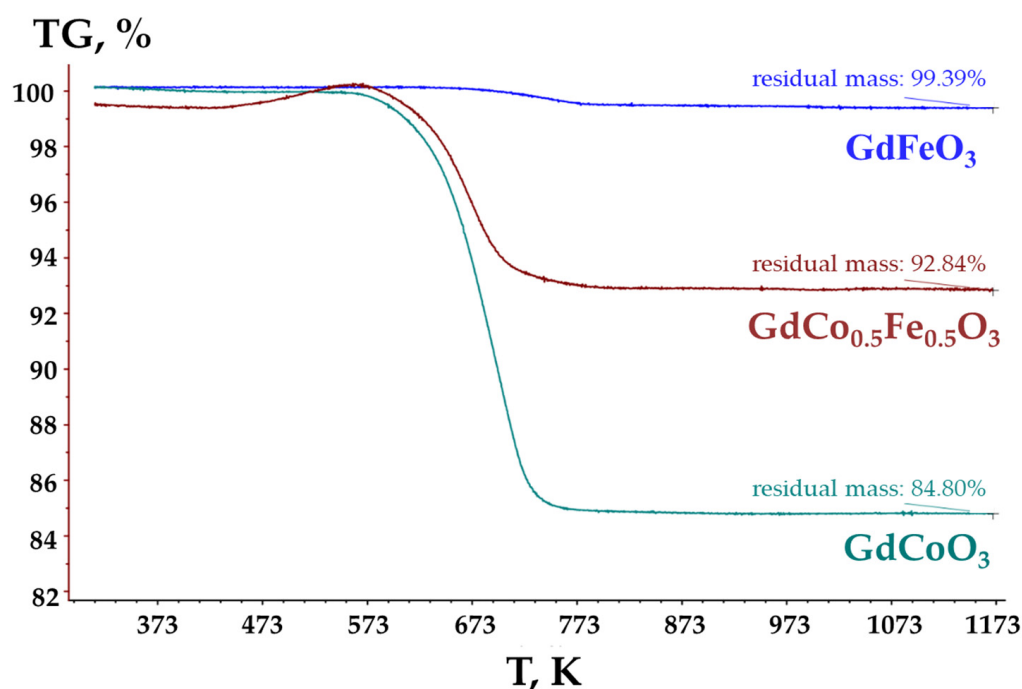


Figure 10. Mass loss curves for GdFeO_3 , $\text{GdCo}_{0.5}\text{Fe}_{0.5}\text{O}_3$ and GdCoO_3 samples.

TG analysis showed a loss of mass of the samples up to temperatures of ~893–913 K (620–640 °C). The amount of deposited carbon increases with increasing cobalt content. The largest amount was observed in GdCoO_3 . However, for all investigated perovskite systems, the formation of the so-called “resin” as well as the “encapsulation” of the catalyst particles was not observed.

3. Materials and Methods

3.1. Catalyst Preparation

The synthesis of $\text{GdCo}_x\text{Fe}_{1-x}\text{O}_3$ complex oxides ($x = 0; 0.2; 0.5; 0.8; 1$) was performed using the citrate-nitrate sol-gel technique [40,41]. Stoichiometric $\text{Gd}(\text{NO}_3)_3 \cdot 6\text{H}_2\text{O}$ (99.9%, Vecton, St. Petersburg, Russia), $\text{Fe}(\text{NO}_3)_3 \cdot 9\text{H}_2\text{O}$ (98%, Vecton, St. Petersburg, Russia) и $\text{Co}(\text{NO}_3)_3 \cdot 9\text{H}_2\text{O}$ (98.5%, Vecton, St. Petersburg, Russia) nitrates were dissolved in

distilled water, and then the flask was placed on a magnetic stirrer with a thermostat. Citric acid was added to the resulting salt solution with constant stirring. After the complete dissolution of citric acid, to set the pH of the solution at 6, an ammonia solution was added, and then the solution was evaporated at a temperature of ~ 120 °C until the resulting gel ignited and a black powder was formed. Then the temperature was raised to 450 °C and the resulting powder was calcined for 2 h. The samples containing cobalt were additionally calcined at 800 °C for 1 h.

3.2. Characterization

Powder X-ray diffraction (XRD) was used to determine the phase composition and structural data of the obtained compounds. The analysis was carried out using a Rigaku MiniFlex II diffractometer with $\text{CuK}\alpha$ radiation. Diffraction patterns of all investigated compounds were obtained under the same conditions sufficient to detect all characteristic reflections: the range of angles is $2\theta = 10\text{--}60^\circ$, and the scanning speed is $5^\circ/\text{min}$. The obtained diffraction patterns were analyzed by comparing the present reflections with the data of the ICDD-PDF2 database. The data obtained allowed us to conclude the phase composition of the studied compounds.

X-ray photoelectron spectroscopy (XPS) was used to analyze the surface composition and determine the state of atoms. The measurements were carried out on a Thermo Fisher Scientific Escalab 250Xi spectrometer using radiation $\text{AlK}\alpha = 1486.6$ eV, spectral resolution-0.5 eV. The characteristic C1s line (C-C bond), which is observed at a bond energy of 284.8 eV, was used as a control line. Experiments on temperature-programmed hydrogen reduction (H_2 -TPR) were carried out on a Micromeritics AutoChem II 2920 analyzer. Samples with a mass of <0.05 g were placed in a U-shaped quartz reactor and heated with a constant flow of a gas mixture (10% H_2 /90% Ar, feed rate = 50 mL/min) up to 1000 °C (heating rate = 10 °C/min). The amount of absorbed gas was measured using a thermal conductivity detector (TCD). In order to exclude the effect of water vapor on the operation of the TCD, a trap was placed in front of the detector and in a Dewar with ethyl alcohol ($T = -139$ °C). Sample temperature, valve position and gas flow rate data were monitored and controlled using a computer equipped with Micromeritics AutoChem II software.

Thermogravimetric analysis using a Netzsch STA 449 F5 Jupiter was performed to estimate the amount of deposited carbon after catalytic tests. The studies were carried out on samples with a suspension of 20–30 mg in a stream of air (rate = 50 mL/min⁻¹) at a heating rate of 10 K/min⁻¹ in the temperature range 303–1173 K. The specific surface area was determined by the method of low-temperature nitrogen adsorption at $T = 77$ K on Nova 4200e (Quantachrome, Boynton Beach, FL, USA) and QuadrasorbSI devices. The samples were preliminarily degassed at 300 °C for 5 h. The obtained adsorption-desorption isotherms were used to estimate the specific surface area of the samples by applying the BET method.

3.3. Catalytic Activity Tests

Catalyst performance of the samples in the carbon monoxide hydrogenation reaction was evaluated in a quartz tubular microreactor containing 0.1 g of the sample diluted in 0.5 g of quartz in order to avoid the formation of hot spots in the catalytic bed alongside increasing the volume. Activity tests were carried out in the temperature range 523–708 K under atmospheric pressure with the feed composition $\text{CO}:\text{H}_2 = 1:2$ and total flow rate of 1.5 L·h⁻¹, which corresponds to GHSV of 8700 h⁻¹. Gaseous effluent was analyzed online using a gas chromatograph instrument (Crystal 5000.2, a column of stainless steel filled with Porapack Q, argon as a carrier gas) fitted with thermal conductivity and flame ionization detectors.

The catalytic characteristics were calculated using the following equations:

$$X_i, \% = \frac{n_{int} - n_{out}}{n_{int}} \times 100 \quad (4)$$

$$S_i = \frac{R_i}{\sum R_i} \cdot 100\%, \quad (5)$$

$$R_i = \frac{n_{iout}\omega}{Vm} \quad (6)$$

where n_{int} и n_{out} is the initial amount of substance and mole yield of products, $\sum n_i$ is the mole yield of hydrocarbon reaction products (mole), R_i is the rate of formation of the i -th reaction product per 1 g catalyst (mol/h·g), $\sum R_i$ is the sum of yields of the i -th reaction products per 1 g catalyst (mol/h·g), ω is volumetric rate of the reaction mixture (L/h), V is the volume of the chromatograph loop (0.153×10^{-3} L) and m is the mass of the catalyst, g.

The carbon chain growth factor α_i was calculated using Equation (7) [42]:

$$\alpha_i = \frac{\sum_{k>i} \frac{Y_k}{k}}{\sum_{k \geq i} \frac{Y_k}{k}} \quad (7)$$

where α_i is carbon chain growth factor for the intermediate with the number of carbon atoms I , Y_k is the yield of the component with the number of carbon atoms k .

The coefficient α_1 is the probability of the addition of CO to the intermediate containing one carbon atom to form an intermediate with two carbon atoms; α_2 is the probability of the next step of the addition of CO to the intermediate with two carbon atoms, etc.

4. Conclusions

Complex perovskite-type oxides $\text{GdCo}_x\text{Fe}_{1-x}\text{O}_3$ ($x = 0; 0.2; 0.5; 0.8; 1.0$) prepared by the sol-gel method were studied as catalysts for the hydrogenation of carbon monoxide. The effect of iron substitution by cobalt on the physicochemical and catalytic properties in the process was investigated. It was found that the metals in the samples were in heterovalent states $\text{Fe}^{2+}/\text{Fe}^{3+}$ and $\text{Co}^{2+}/\text{Co}^{3+}$, which is compensated by oxygen vacancies. It was found that the partial substitution of iron for cobalt in $\text{GdCo}_x\text{Fe}_{1-x}\text{O}_3$ ($0.5 < x < 1$) and a decrease in the Co^{2+} share in the sample resulted in an increase in CO conversions; nevertheless, $x = 0.2$ with the maximum $\text{Co}^{2+}/\sum \text{Co}^{n+}$ ratio and minimum $\text{Fe}^{2+}/\sum \text{Fe}^{n+}$ ratio was the most selective for ethylene. It has been suggested that Co^{3+} and Fe^{3+} are active centers, while the presence of Co^{2+} somewhat complicates the process and shifts it towards the formation of olefins. It was also found that varying the composition of $\text{GdCo}_x\text{Fe}_{1-x}\text{O}_3$ complex oxides leads to changes in the oxygen-metal bond energy in Gd-O-Me, the ratio of metals in different oxidation states, and the amount of surface and lattice oxygen, which is reflected in the adsorption and catalytic characteristics of complex oxides and change of the quantitative ratio of olefins in the process of CO hydrogenation.

Author Contributions: Conceptualization and methodology, I.A.Z. and T.F.S.; investigation, E.M.B., T.A.K. and L.V.Y.; data curation, T.A.K.; writing—original draft, E.M.B., L.V.Y. and T.A.K. writing—review and editing, T.A.K., T.F.S. and I.A.Z.; supervision, A.G.C.; project administration, A.G.C. All authors have read and agreed to the published version of the manuscript.

Funding: This publication was supported by the RUDN University Scientific Projects Grant System, project № 021521-2-174 and the scholarship of the President of the Russian Federation (№ CII-686.2021.1).

Data Availability Statement: The original data are available from E.M.B. and L.V.Y.

Acknowledgments: Authors are also grateful to Saint Petersburg State University Research Park. The XRD study was carried out at the Research Center for X-ray Diffraction Studies and was performed at the Resource Center for Studies in Surface Science. The TG analysis was carried out in the Center of Thermal Analysis and Calorimetry.

Conflicts of Interest: The authors declare no conflict of interest. The funders played no role in the design of the study; in the collection, analysis or interpretation of data; in the writing of the manuscript or in the decision to publish the results.

References

1. Brussino, P.; Banús, E.D.; Ulla, M.A.; Bortolozzi, J.P. NiO-based ceramic structured catalysts for ethylene production: Substrates and active sites. *Catal. Today* **2022**, *383*, 84–92. [CrossRef]
2. Coomb, D. EVP, Global Olefins & Polyolefins, Chemical Intensity Conference. 2016. Available online: <https://www.lyondellbasell.com/globalassets/investors/events/2016/160314-lyb-gs-chemical-intensity-conference-final.pdf> (accessed on 15 March 2016).
3. Gao, Y.; Jiang, J.; Meng, Y.; Yan, F.; Aihemaiti, A. A review of recent developments in hydrogen production via biogas dry reforming. *Energy Convers. Manag.* **2018**, *171*, 133–155. [CrossRef]
4. Takanabe, K.; Nagaoka, K.; Nariai, K.; Aika, K. Influence of reduction temperature on the catalytic behavior of Co/TiO₂ catalysts for CH₄/CO₂ reforming and its relation with titania bulk crystal structure. *J. Catal.* **2005**, *230*, 75–85. [CrossRef]
5. Fan, X.; Liu, Z.; Zhu, Y.A.; Tong, G.; Zhang, J.; Engelbrekt, C.; Ulstrup, J.; Zhu, K.; Zhou, X. Tuning the composition of metastable Co_xNi_yMg_{100-x-y}(OH)(OCH₃) nanoplates for optimizing robust methane dry reforming catalyst. *J. Catal.* **2015**, *330*, 106–119. [CrossRef]
6. Seiyama, T. Total Oxidation of Hydrocarbons on Perovskite Oxides. *Catal. Rev.* **1992**, *34*, 281–300. [CrossRef]
7. Voorhoeve, R.J.H.; Johnson, D.W., Jr.; Remeika, J.P.; Gallagher, P.K. Perovskite oxides: Materials science in catalysis. *Science* **1977**, *195*, 827–833. [CrossRef] [PubMed]
8. Singh, U.G.; Li, J.; Bennett, J.W.; Rappe, A.M.; Seshadri, R.; Scott, S.L. A Pd-doped perovskite catalyst, BaCe_{1-x}Pd_xO₃, for CO oxidation. *J. Catal.* **2007**, *249*, 349–358. [CrossRef]
9. Bashan, V.; Ust, Y. Perovskite catalysts for methane combustion: Applications, design, effects for reactivity and partial oxidation. *Int. J. Energy Res.* **2019**, *43*, 7755–7789. [CrossRef]
10. Saada, Y.; Álvarez-Serrano, I.; López, M.L.; Hidouria, M. Structural and dielectric characterization of new lead-free perovskites in the (SrTiO₃)-(BiFeO₃) system. *Ceram. Int.* **2016**, *42*, 8962–8973. [CrossRef]
11. Giannakas, A.E.; Leontiou, A.A.; Ladavos, A.K.; Pomonis, P.J. Characterization and catalytic investigation of NO + CO reaction on perovskites of the general formula La_xM_{1-x}FeO₃ (M = Sr and/or Ce) prepared via a reverse micelles microemulsion route. *Appl. Catal. A Gen.* **2006**, *309*, 254–262. [CrossRef]
12. Kulkarni, A.S.; Jayaram, R.V. Liquid phase catalytic transfer hydrogenation of aromatic nitro compounds on perovskites prepared by microwave irradiation. *Appl. Catal. A Gen.* **2003**, *252*, 225–230. [CrossRef]
13. Goldwasser, M.R.; Dorantes, V.E.; Pérez-Zurit, M.J.; Sojo, P.R.; Cubeiro, M.L.; Pietri, E.; González-Jiménez, F.; NgLee, Y.; Moronta, D. Modified iron perovskites as catalysts precursors for the conversion of syngas to low molecular weight alkenes. *J. Mol. Catal. A Chem.* **2003**, *193*, 227–236. [CrossRef]
14. Silva-Santana, M.C.; daSilva, C.A.; Barrozo, P.; Plaza, E.J.R.; Valladares, L.d.; Moreno, N.O. Magnetocaloric and magnetic properties of SmFe_{0.5}Mn_{0.5}O₃ complex perovskite. *J. Magn. Magn. Mater.* **2016**, *401*, 612–617. [CrossRef]
15. Kesić, Ž.; Lukić, I.; Zdujčić, M.; Jovalekić, Č.; Veljković, V.; Skala, D. Assessment of CaTiO₃, CaMnO₃, CaZrO₃ and Ca₂Fe₂O₅ perovskites as heterogeneous base catalysts for biodiesel synthesis. *Fuel Process. Technol.* **2016**, *143*, 162–168. [CrossRef]
16. Forni, L.; Rossetti, I. Catalytic combustion of hydrocarbons over perovskites. *Appl. Catal. B Environ.* **2002**, *38*, 29–37. [CrossRef]
17. Galasso, F.S. *Structure of Perovskite-Type Compounds*; A Volume in International Series of Monographs in Solid State Physics; Elsevier Inc.: Amsterdam, The Netherlands, 1969; pp. 3–49. [CrossRef]
18. Moure, C.; Peña, O. Recent advances in perovskites: Processing and properties. *Prog. Solid State Chem.* **2015**, *43*, 123–148. [CrossRef]
19. Royer, S.; Duprez, D.; Can, F.; Courtois, X.; Batiot-Dupeyrat, C.; Laassiri, S.; Alamdari, H. Perovskites as Substitutes of Noble Metals for Heterogeneous Catalysis: Dream or Reality. *Chem. Rev.* **2014**, *114*, 10292. [CrossRef]
20. Lopatin, S.I.; Zvereva, I.A.; Chislova, I.V. Vaporization and Thermodynamic Properties of GdFeO₃ and GdCoO₃ Complex Oxides. *Russ. J. Gen. Chem.* **2020**, *90*, 1495–1500. [CrossRef]
21. Peña, M.A.; Fierro, J.L.G. Chemical Structures and Performance of Perovskite Oxides. *Chem. Rev.* **2001**, *101*, 1981–2018. [CrossRef]
22. Oh, J.H.; Kwon, B.W.; Cho, J.; Lee, C.H.; Kim, M.K.; Choi, S.H.; Yoon, S.P.; Han, J.; Nam, S.W.; Kim, J.Y.; et al. Importance of Exsolution in Transition-Metal (Co, Rh, and Ir)-Doped LaCrO₃ Perovskite Catalysts for Boosting Dry Reforming of CH₄ Using CO₂ for Hydrogen Production. *Ind. Eng. Chem. Res.* **2019**, *58*, 6385–6393. [CrossRef]
23. Wang, H.; Dong, X.; Zhao, T.; Yu, H.; Li, M. Dry reforming of methane over bimetallic Ni-Co catalyst prepared from La(Co_xNi_{1-x})_{0.5}Fe_{0.5}O₃ perovskite precursor: Catalytic activity and coking resistance. *Appl. Catal. B Environ.* **2019**, *245*, 302–313. [CrossRef]
24. Gao, S.; Liu, N.; Liu, J.; Chen, W.; Liang, X.; Yuan, Y. Synthesis of higher alcohols by CO hydrogenation over catalysts derived from LaCo_{1-x}Mn_xO₃ perovskites: Effect of the partial substitution of Co by Mn. *Fuel* **2020**, *261*, 116415. [CrossRef]
25. Zhu, Q.; Cheng, H.; Zou, X.; Lu, X.; Xu, Q.; Zhou, Z. Synthesis, characterization, and catalytic performance of La_{0.6}Sr_{0.4}Ni_xCo_{1-x}O₃ perovskite catalysts in dry reforming of coke oven gas. *Chin. J. Catal.* **2015**, *36*, 915–924. [CrossRef]
26. Bedel, L.; Roger, A.C.; Estournes, C.; Kiennemann, A. Co₀ from partial reduction of La(Co,Fe)O₃ perovskites for Fischer-Tropsch synthesis. *Catal. Today* **2003**, *85*, 207–218. [CrossRef]
27. Bedel, L.; Roger, A.C.; Rehspringer, J.L.; Zimmermann, Y.; Kiennemann, A. La_(1-y)Co_{0.4}Fe_{0.6}O_{3-δ} perovskite oxides as catalysts for Fischer-Tropsch synthesis. *J. Catal.* **2005**, *235*, 279–294. [CrossRef]
28. Bedel, L.; Roger, A.C.; Rehspringer, J.L.; Kiennemann, A. Structure-controlled La-Co-Fe perovskite precursors for higher C₂-C₄ olefins selectivity in Fischer-Tropsch synthesis. *Stud. Surf. Sci. Catal.* **2004**, *147*, 319–324. [CrossRef]

29. Sheshko, T.F.; Markova, E.B.; Sharaeva, A.A.; Kryuchkova, T.A.; Zvereva, I.A.; Chislova, I.V.; Yafarova, L.V. Carbon Monoxide Hydrogenation over Gd(Fe/Mn)O₃ Perovskite-Type Catalysts. *Pet. Chem.* **2019**, *59*, 1307–1313. [[CrossRef](#)]
30. Escalona, N.; Fuentealba, S.; Pecchi, G. Fischer-Tropsch synthesis over LaFe_{1-x}Co_xO₃ perovskites from a simulated biosyngas feed. *Appl. Catal. A Gen.* **2010**, *381*, 253–260. [[CrossRef](#)]
31. Ding, M.; Yang, Y.; Wu, B.; Li, Y.; Wang, T.; Ma, L. Study on reduction and carburization behaviors of iron phases for iron-based Fischer-Tropsch synthesis catalyst. *Energy Proc.* **2014**, *61*, 2267–2270. [[CrossRef](#)]
32. Sheshko, T.F.; Kryuchkova, T.A.; Yafarova, L.V.; Borodina, E.M.; Serov, Y.M.; Zvereva, I.A.; Cherednichenko, A.G. Gd-Co-Fe perovskite mixed oxides as catalysts for dry reforming of methane. *Sustain. Chem. Pharm.* **2022**, *30*, 100897. [[CrossRef](#)]
33. Yafarova, L.V.; Mamontov, G.V.; Chislova, I.V.; Silyukov, O.I.; Zvereva, I.A. The Effect of Transition Metal Substitution in the Perovskite-Type Oxides on the Physicochemical Properties and the Catalytic Performance in Diesel Soot Oxidation. *Catalysts* **2021**, *11*, 1256. [[CrossRef](#)]
34. Sheshko, T.F.; Serov, Y.M.; Kryuchkova, T.A.; Khayrullina, I.A.; Chislova, I.V.; Yafarova, L.V.; Zvereva, I.A. Study of effect of preparation method and composition on the catalytic properties of complex oxides (Gd,Sr)_{n+1}Fe_nO_{3n+1} for dry reforming of methane. *Nanotechnol. Russ.* **2017**, *12*, 174–184. [[CrossRef](#)]
35. Wu, Y.; Li, L.; Chu, B.; Yi, Y.; Qin, Z.; Fan, M.; Qin, Q.; He, H.; Zhang, L.; Dong, L.; et al. Catalytic reduction of NO by CO over B-site partially substituted LaM_{0.25}Co_{0.75}O₃ (M = Cu, Mn, Fe) perovskite oxide catalysts: The correlation between physicochemical properties and catalytic performance. *Appl. Catal. A Gen.* **2018**, *568*, 43–53. [[CrossRef](#)]
36. Merino, N.A.; Barbero, B.P.; Eloy, P.; Cadús, L.E. La_{1-x}Ca_xCoO₃ perovskite-type oxides: Identification of the surface oxygen species by XPS. *Appl. Surf. Sci.* **2006**, *253*, 1489–1493. [[CrossRef](#)]
37. Wang, Y.; Ren, J.; Wang, Y.; Zhang, F.; Liu, X.; Guo, Y.; Lu, G. Nanocasted synthesis of mesoporous LaCoO₃ perovskite with extremely high surface area and excellent activity in methane combustion. *J. Phys. Chem. C* **2008**, *112*, 15293–15298. [[CrossRef](#)]
38. Sun, J.; Zhao, Z.; Li, Y.; Yu, X.; Zhao, L.; Li, J.; Wei, Y.; Liu, J. Synthesis and catalytic performance of macroporous La_{1-x}Ce_xCoO₃ perovskite oxide catalysts with high oxygen mobility for catalytic combustion of soot. *J. Rare Earths Chin. Soc. Rare Earths* **2020**, *38*, 584–593. [[CrossRef](#)]
39. Kryuchkova, T.A.; Kost', V.V.; Sheshko, T.F.; Chislova, I.V.; Yafarova, L.V.; Zvereva, I.A. Effect of Cobalt in GdFeO₃ Catalyst Systems on Their Activity in the Dry Reforming of Methane to Synthesis Gas. *Pet. Chem.* **2020**, *60*, 609–615. [[CrossRef](#)]
40. Chislova, I.V.; Matveeva, A.A.; Volkova, A.V.; Zvereva, I.A. Sol-gel synthesis of nanostructured perovskite-like gadolinium ferrites. *Glass Phys. Chem.* **2011**, *37*, 653–660. [[CrossRef](#)]
41. Yafarova, L.V.; Chislova, I.V.; Zvereva, I.A.; Kryuchkova, T.A.; Kost, V.V.; Sheshko, T.F. Sol-gel synthesis and investigation of catalysts on the basis of perovskite-type oxides GdMO₃ (M = Fe, Co). *J. Sol. Gel Sci. Technol.* **2019**, *92*, 264–272. [[CrossRef](#)]
42. Osman, M.E.; Maximov, V.V.; Dorokhov, V.S.; Mukhin, V.M.; Sheshko, T.F.; Kooyman, P.J.; Kogan, V.M. Carbon-Supported KCoMoS₂ for Alcohol Synthesis from Synthesis Gas. *Catalysts* **2021**, *11*, 1321. [[CrossRef](#)]

Disclaimer/Publisher's Note: The statements, opinions and data contained in all publications are solely those of the individual author(s) and contributor(s) and not of MDPI and/or the editor(s). MDPI and/or the editor(s) disclaim responsibility for any injury to people or property resulting from any ideas, methods, instructions or products referred to in the content.